Hydrogen dissociation on metal surfaces

Wijzenbroek, M.

CHAPTER 5

Towards a specific reaction parameter density functional for reactive scattering of H_2 from Pd(111)

This chapter is based on:

J. M. Boereboom, M. Wijzenbroek, M. F. Somers, and G. J. Kroes. Towards a specific reaction parameter density functional for reactive scattering of H_2 from Pd(111). *Journal of Chemical Physics* **139**(24), 244707, 2013.

Abstract

Recently, an implementation of the specific reaction parameter (SRP) approach to density functional theory (DFT) was used to study several reactive scattering experiments of H_2 on Cu(111). It was possible to obtain chemical accuracy (1 kcal/mol $\approx$ 4.2 kJ/mol), and therefore, accurately model the dissociation of hydrogen on an activated metal surface. In this work, the SRP-DFT methodology is applied to the dissociation of hydrogen on a Pd(111) surface, in order to test whether the SRP-DFT approach is also applicable to non-activated systems. In the calculations, the Born–Oppenheimer and static surface (BOSS) approximations are used. A comparison to molecular beam sticking experiments on H_2/Pd(111) suggested the PBE-vdW-DF functional as a candidate exchange–correlation functional describing the reactive scattering of H_2 on Pd(111), because at high incidence energies simulated molecular beam reaction probabilities obtained with the quasi-classical trajectory (QCT) method and using a PBE-vdW-DF potential energy surface are in good agreement with experimental sticking probabilities. Unfortunately, quantum dynamics calculations are not able to reproduce the molecular beam sticking results for low incidence energies. From a comparison to initial state-resolved (degeneracy averaged) sticking probabilities it seems clear that for H_2/Pd(111) dynamic trapping and steering effects are important, which are not yet well modelled with the potential energy surfaces (PESs) considered here. Applying the SRP-DFT method to systems where H_2 dissociation is non-activated remains difficult. It is suggested that a density functional that yields a broader barrier distribution than PBE-vdW-DF (*i.e.*, non-activated dissociation at some sites but similarly high barriers at the high energy end of the spectrum) could allow a more accurate description of the available experiments.

5.1 Introduction

A large number of chemical reactions involve gas–surface interactions. These interactions are of great importance to the chemical industry, where heterogeneous catalysis lies at the heart of the synthesis of many

important compounds.[1] One famous example is the Haber–Bosch process, which is arguably the most important invention of the twentieth century.[2] This process is the main industrial route to produce ammonia, which is used in fertilizers. The dissociative chemisorption of hydrogen on metal surfaces is one of the most fundamental gas–surface reactions. Heterogeneously catalysed processes typically involve several of such elementary surface reaction steps.[3,4]

Unfortunately, it is difficult to accurately model the dissociation of hydrogen on metal surfaces.[5] In order to correctly calculate the reaction probability of hydrogen dissociation on a metal surface, one needs to obtain reaction barriers with chemical accuracy (1 kcal/mol ≈ 4.2 kJ/mol).[6] Currently, the electronic structure method of choice to study the dissociation of H_2 on a metal surface is density functional theory (DFT),[7] with functionals based on the generalized gradient approximation (GGA). Even these calculations, however, have mean absolute errors of at best 4 kcal/mol, for gas-phase reaction barrier heights[8,9] (unfortunately, for molecule–surface reactions such systematic investigations are currently not available).[10] In contrast, high accuracy for gas-phase reactions is available from high-level *ab initio* theory, and to a lesser extent from DFT with hybrid functionals.[8,9] The scaling of such methods, however, is rather unfavourable, so that in practice these methods cannot yet be applied to the computation of global potential energy surfaces (PESs) for molecule–surface reactions. Therefore, recently an implementation[6] of the specific reaction parameter (SRP) approach to DFT,[11,12] adapted to molecule–surface reactions, was proposed. This allowed a quantitative description of several reactive scattering experiments of H_2 on Cu(111), which is a benchmark system for activated hydrogen–metal surface reactions.[6] It was shown that this SRP exchange–correlation (XC) functional was also transferable to the H_2/Cu(100) reaction.[13]

In calculations on H_2 dissociation on Cu(111),[6] a SRP XC functional was constructed in the following way,

$$E_{XC}^{SRP} = \alpha E_{XC}^{1} + (1 - \alpha) E_{XC}^{2}. \tag{5.1}$$

Here, the energy of the SRP XC functional can be written as a linear combination of E_{XC}^{1} and E_{XC}^{2}, the energy expression of any two arbitrary

XC functionals. The essence of the SRP approach to DFT is that an XC functional is found (possibly through an empirical fit) that yields an excellent agreement with the sticking probability measured in molecular beam experiments, with the desired result that also other, more detailed observables (like diffraction probabilities) are described well. Therefore, the SRP XC functional need not be a mix of two XC functionals. The question remains, however, if the approach first tested and found to work well for activated hydrogen–metal systems (*i.e.*, fitting an XC functional by demanding that dynamics calculations performed with the Born–Oppenheimer static surface (BOSS) model on a PES obtained from DFT calculations reproduce molecular beam sticking probability measurements) is also appropriate to model H_2 dissociation in non-activated systems. In this work, the specific reaction parameter methodology will be applied to the dissociation of hydrogen on a Pd(111) surface, in order to test whether the SRP approach is applicable to non-activated systems as well.

Several molecular beam experiments have been performed by the Rendulic group on the sticking of H_2 on Pd(111).[14–17] Furthermore, molecular beam experiments have been performed for this system by Gostein and Sitz,[18] who analysed their results to extract initial state-resolved reaction probabilities.

Unfortunately, there are large discrepancies between the sticking probabilities obtained from the different molecular beam studies. In figure 5.1, the molecular beam sticking probabilities for all the available experiments are plotted. It can be seen that there is a large spread in the experimental data of the molecular beam experiments by the group of Rendulic. From private correspondence,[19] it becomes clear that the latest experiment (exp. Rendulic 2001[16,17]) is probably the most reliable. This experiment is also in reasonably good agreement with the rotationally averaged sticking coefficients obtained by Gostein and Sitz.[18]

Apart from experimental work on the dissociation of hydrogen on Pd(111), this system has also been studied theoretically.[20–28] The theoretical work mainly focused on rotational effects on the dissociation of hydrogen on Pd(111), and on the role zero-point energy (ZPE) plays in the classical dynamics of H_2 dissociation. Surface temperature effects

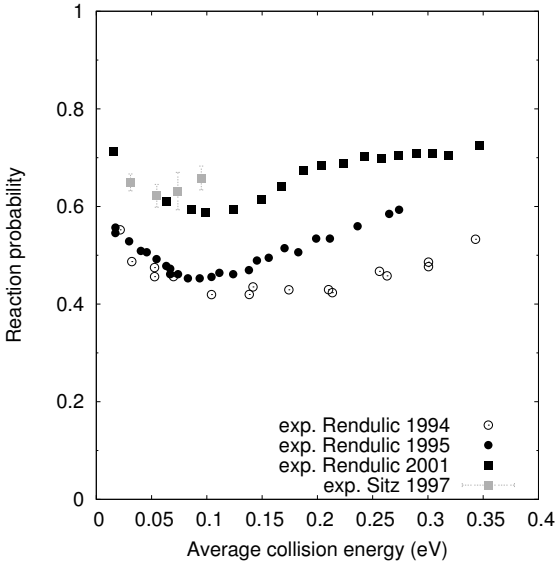

Figure 5.1 Molecular beam sticking probabilities for all the available experiments. The experiment by Resch *et al.*[14] is labelled exp. Rendulic 1994, the experiment by Beutl *et al.*[15] is labelled exp. Rendulic 1995, and the experiment performed by Lesnik[16] and Beutl *et al.*[17] is labelled exp. Rendulic 2001. The experiment by Gostein and Sitz[18] is labelled exp. Sitz 1997.

have also been considered.[27,28] In these studies it was found that energy exchange can promote trapping of the H_2 near the surface, and thereby reaction (trapping mediated reaction). There have also been a few studies which focused on the scattering of H_2 from Pd(111),[29,30] but in this work scattering processes will not be discussed. Also other low index surfaces have been studied intensively. Experimental data is available for Pd(100)[31–34] and Pd(110),[35] and theoretical studies have also been performed on Pd(100)[36–40] and Pd(110).[35,41–43]

This chapter is organized as follows: in section 5.2, the methods used to obtain the PES and to carry out the dynamics calculations in this work are presented. The computational details are also discussed there. The results and discussion can be found in section 5.3, where first the PESs is discussed in section 5.3.1, after which a candidate for the specific reaction parameter XC functional is discussed in section 5.3.2. For this candidate functional, quantum dynamics (QD) calculations

have been performed, and are compared with results obtained with the quasi-classical trajectory (QCT) method and experiment. This comparison is done for both molecular beams (section 5.3.2) and initial state-specific reaction probabilities (section 5.3.3). The main conclusions will be summarized and presented in section 5.4.

5.2 Methods

5.2.1 Born–Oppenheimer static surface model

In this work the BOSS model has been used. Within this model the H_2–surface system is treated using six molecular degrees of freedom, by freezing the positions of the surface atoms in their ideal lattice positions. The coordinate system used to describe the position and orientation of the molecule with respect to the surface can be found in figure 5.2(a). Here, X, Y, and Z are the center of mass coordinates of H_2, r is the H–H distance, ϑ is the polar angle of the molecular axis with the Z-axis, and φ is the azimuthal angle. In the BOSS model electron–hole (e–h) pair excitation and phonons are neglected. Reactive scattering calculations on H_2/Pt(111) using a single PES and neglecting e–h pair excitation were able to describe the dissociation and diffractive scattering of hydrogen on Pt(111) accurately.[44] Moreover, calculations on H_2/Cu(111),[45] Cu(110),[46] and Ru(0001)[47] modelling e–h pair excitation with friction coefficients showed very small non-adiabatic energy losses. These results suggest that non-adiabatic effects are not important when modelling H_2–metal surface systems, supporting the validity of the Born–Oppenheimer approximation for these systems.

The validity of the static surface approximation has been tested by static surface QCT calculations on the reactive scattering of D_2 from Cu(111) at low surface temperature ($T_s = 120$ K).[6,48] These calculations were in good agreement with *ab initio* molecular dynamics (AIMD) results,[49] which modelled phonon motion. Also results obtained with the static corrugation model (SCM) in chapter 3, which excluded energy exchange with the surface but included the displacement of surface atoms, were in good agreement with the results above for low surface temperatures. These studies suggested that, for high surface temper-

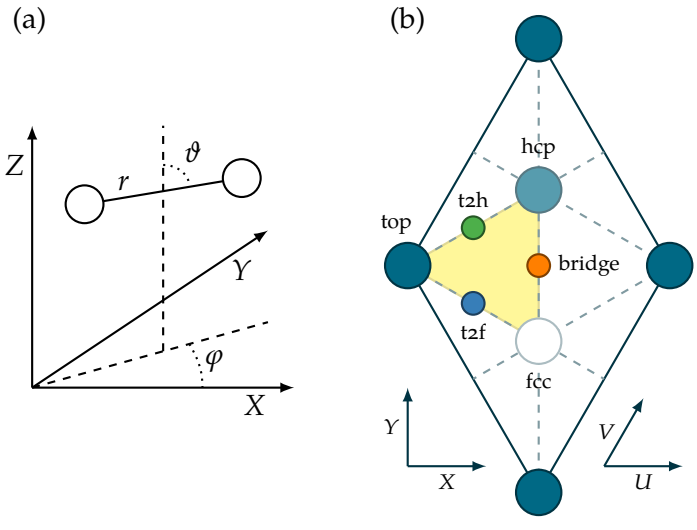

Figure 5.2 (a) Coordinate system for dissociation of H_2 on a surface. In the plot, X, Y, and Z are the center of mass coordinates of H_2, r is the H–H distance, ϑ is the polar angle of the molecular axis with the Z-axis, and φ is the azimuthal angle. (b) Schematic representation of the unit cell with the high symmetry sites on the Pd(111) surface, and of considered H_2–surface geometries.

atures, thermal expansion of the surface can be important, which has been tested recently.[50]

5.2.2 Electronic structure method

To construct 6D PESs, plane wave DFT calculations were performed for H/Pd(111) and H_2/Pd(111) with version 5.2.12 of the VASP[51–54] software package. The surface is modelled by a five layer slab representation[55,56] using a 2 × 2 supercell.[57] Each PES has p3m1 symmetry.[58] As a consequence, a distinction can be made between second and third layer hollow sites, called HCP and FCC respectively, which are shown in figure 5.2(b). PESs have been calculated for four different XC functionals: PBE,[59] RPBE,[60] PBE-vdW-DF,[59,61] and PBEα-vdW-DF.[61,62] In the PBEα-vdW-DF functional, $\alpha = 0.5$ is chosen. In the PBEα method α is defined in such a way that $\alpha = 1$ corresponds to PBE, and $\alpha = \infty$ corresponds to RPBE.[62] For PBE-vdW-DF and PBEα-vdW-DF, the

PBE correlation is replaced by vdW-DF correlation[61] resulting in PBE and PBEα exchange and vdW-DF correlation. In VASP the vdW-DF method uses[63] the method of Román-Pérez and Soler.[64] The lattice constants have been calculated using a plane wave energy cutoff of 450 eV, sampling the Brillouin zone by a $20 \times 20 \times 20$ Γ-centered k-point mesh. Subsequently, a five layer slab was optimized, with the same energy cutoff, and with a $20 \times 20 \times 1$ Γ-centered k-point mesh to sample the Brillouin zone. Each PES is based on more than 6000 single DFT points. These single points are calculated using a plane wave cut-off of 400 eV, and using a $9 \times 9 \times 1$ Γ-centered k-point mesh to sample the Brillouin zone. Convergence tests suggested that the error made in the single DFT points, due to the basis set size and numerical integration, is around 5 meV. The PBE and RPBE functionals from LibXC[65] version 1.2.0 were used. To describe the core electrons, the projector augmented wave (PAW) method[66,67] has been used for PBE-vdW-DF and PBEα-vdW-DF. For PBE and RPBE ultrasoft pseudopotentials (USPPs) have been used.[68,69]

5.2.3 PES interpolation

The 6D PESs were constructed in a way analogous to that described in section 4.2.2. In total, 29 2D PESs were used in the interpolation procedure for the molecule–surface PES. The 2D PESs are a function of Z and r, and represent the most important configurations of the H_2 molecule interacting with Pd(111). Each 2D PES is based on a cubic spline interpolation of 196 points (14 in r and 14 in Z) which are calculated with DFT. The positions (X, Y) and orientation (ϑ, φ) of H_2 in the 2D cuts can be found in table 4.1. A very important task is to interpolate the 2D PESs to obtain an accurate 6D PES. Due to the strong corrugation of the potential near the surface, a direct interpolation can lead to large errors in the interpolated PES.[70] The corrugation reducing procedure (CRP) method,[21,71] as discussed in section 2.1.1 has therefore been used.The required 1D PESs representing the H–surface interaction were calculated for 10 different sites (table 4.2).

5.2.4 Dynamics methods

QCT calculations for each initial (v, J) state were performed for 14 normal incidence energies, spread equidistantly over a normal incidence energy interval of $25 - 350$ meV. The used QCT method has been described in section 2.3 of this thesis. Initially, the center of mass of the hydrogen molecule is placed at a distance of 7 Å from the surface. It is assumed that dissociation occurs when r (the H–H distance) exceeds 2.25 Å. Scattering is assumed to have occurred when the hydrogen molecule has a momentum away from the surface, and a hydrogen–surface distance larger than 7 Å is reached. To obtain statistically accurate results for each point at least 10^4 trajectories were computed, which are sampled equally over the possible m_J states.

The QD calculations have been carried out using a time-dependent wave packet (TDWP) method[72,73] as described in section 2.4. In order to cover a large range of normal incidence energies ($40-600$ meV) two calculations are performed with separate energy ranges: $40-200$ meV and $150 - 600$ meV. This is done to avoid problems which may arise from the interaction of the optical potential with the low energy components in the wave packet, if only one broad Gaussian initial wave packet is used to cover the entire range from $40 - 600$ meV.[73]

5.2.5 Computation of observables

Initial state-resolved reaction probabilities and molecular beam sticking probabilities were computed as discussed in section 2.5. In order to compare the computed sticking probabilities with molecular beam experiments from the Rendulic group, the parameters v_0 and α (see also equation (2.39)), characterizing the molecular beam, are needed. Unfortunately, for the molecular beam experiments on Pd(111)[14–17] no time-of-flight (TOF) spectra were published. Therefore, the parameters are obtained from experiments with pure beams on H_2 scattering from Cu(111), which were performed by Berger *et al.* in the group of Rendulic. The TOF intensities $G(t; T_n)$ characterizing the H_2 beams are presented in figure 4.4 from the thesis by Berger[74] for T_n = 100, 300, 500, 800, 1100, 1400, and 1700 K. This figure was digitized and fitted[75] according

Table 5.1 Parameters used to simulate the molecular beam experiments. The parameters were obtained by digitizing and fitting figure 4.4 from the thesis by Berger[74] according to equation (5.2). In order to simulate the molecular beam sticking probabilities (equation (2.38)) these parameters enter the flux weighted velocity distribution (equation (2.39)).

T_n (K)	$\langle E_i \rangle$ (eV)	v_0 (m/s)	α (m/s)
100	0.035	1820.7	78.7
300	0.068	2503.9	237.6
500	0.126	3162.2	781.7
800	0.150	3300.1	1007.3
1100	0.240	3691.5	1694.6
1400	0.391	3510.8	2897.2
1700	0.445	3096.6	3411.0

to,

$$G(t; T_n) = c_1 + c_2 \cdot {v_i}^4 \exp\left[-\left(\frac{v_i - v_0}{\alpha}\right)^2\right], \tag{5.2}$$

where c_1 and c_2 are constants. The parameters obtained from the fits are presented in table 5.1. Note that reference 6 only presented parameters for $T_n \geq 1100$ K.

5.2.6 Computational details

The relevant input parameters for the QD calculations are listed in table 5.2. For both energy ranges ($40 - 200$ meV and $150 - 600$ meV) the same input parameters could be used. For the low energy range the convergence errors are lower than for the high energy range (errors of the order of 1% for low incidence energies, and not more than 2% for the high energy range). A long propagation time is needed, due to a chemisorption well in front of the barrier. The wave function is propagated long enough to ensure that the norm of the wave function which is still on the grid at the end of the calculation is no more than 0.01. The total propagation time ranges from 60×10^3 to 360×10^3 a.u.

Table 5.2 Input parameters for the quantum dynamical calculations of H_2 dissociating on Pd(111). For a detailed description of the parameters, see reference 73. For both energy ranges the same input parameters could be used. The values are listed for the calculations with J even, when the calculations with J odd have different parameters they are listed in parentheses. All values are given in atomic units.

Parameter	Description	Value
$N_X = N_Y$	no. of grid points in X and Y	24
N_Z	no. of grid points in Z	128
$N_{Z(\mathrm{sp})}$	no. of specular grid points	240
ΔZ	spacing of Z grid points	0.135
Z_{min}	minimum value of Z	-1.0
N_r	no. of grid points in r	32
Δr	spacing of r grid points	0.25
r_{min}	minimum value of r	0.4
$\mathrm{j}_{\mathrm{max}}$	maximum J value in basis set	18(19)
$m_{\mathrm{j}_{\mathrm{max}}}$	maximum m_J value in basis set	18(19)
Δt	time step	2.5
Z_0	center of initial wave packet	16.64
Z_∞	location of analysis line	12.5
$Z^{\mathrm{opt}}_{\mathrm{start}}$	start of optical potential in Z	12.5
$Z^{\mathrm{opt}}_{\mathrm{end}}$	end of optical potential in Z	16.145
A_Z	strength optical potential in Z	0.0041
$r^{\mathrm{opt}}_{\mathrm{start}}$	start of optical potential in r	4.4
$r^{\mathrm{opt}}_{\mathrm{end}}$	end of optical potential in r	8.15
A_r	strength optical potential in r	0.005
$Z(\mathrm{sp})^{\mathrm{opt}}_{\mathrm{start}}$	start of optical potential in $Z(\mathrm{sp})$	22.22
$Z(\mathrm{sp})^{\mathrm{opt}}_{\mathrm{end}}$	end of optical potential in $Z(\mathrm{sp})$	31.265
$\mathrm{A}_{Z(\mathrm{sp})}$	strength optical potential in $Z(\mathrm{sp})$	0.0041

Table 5.3 The lattice constants (in angstrom), and the first and second interlayer spacings (in Å) for all four computed PESs. Note that the experimental value for the lattice constant is obtained at 4.2 K, whereas the calculations assume a surface temperature of 0 K.

	Lattice constant	d_{1-2}	d_{2-3}
PBE	3.966	2.289	2.281
PBE-vdW-DF	3.996	2.313	2.304
RPBE	4.007	2.311	2.300
PBEα-vdW-DF	3.968	2.294	2.284
Experiment[77]	3.872	–	–

5.3 Results and discussion

5.3.1 Potential energy surface

In table 5.3, the lattice constants and interlayer spacings, computed through energy minimization with DFT, can be found for the four different XC functionals investigated. All the computed lattice constants were converged within 0.003 Å. From the table, it becomes apparent that the calculations overestimate the lattice constant of palladium. In general, GGA functionals cannot give both correct accurate atomic exchange energies, and accurate bond lengths.[76] Since for gas-phase molecules (where GGA functionals are most applied) accurate atomic exchange energies are more important than the precise bond length, GGA functionals typically overestimate the lattice constant. Because the slab relaxations are performed with five layers, the 1st and 4th, and the 2nd and 3rd interlayer spacings are almost identical to one another. Note that justifications of the use of symmetrized slabs are given in reference 50. Test calculations with slabs consisting of up to ten layers confirmed that the interlayer spacings were well converged (discrepancy at most 0.004 Å).

In figure 5.3, four relevant 2D cuts of the PES are shown for the PBE-vdW-DF functional. The top and t2f sites can have both an early and a late barrier, whereas the bridge and FCC sites are early barrier sites. In table 5.4, the corresponding barriers for dissociation of H_2 on Pd(111), relative to the gas-phase minimum, are given for these configurations

Table 5.4 The energy barriers (in meV) for the dissociation of H_2 on Pd(111) relative to the gas-phase minimum are given for four different PESs. The configurations which are listed here are the top ($\vartheta = 90°$, $\varphi = 0°$) site, the bridge ($\vartheta = 90°$, $\varphi = 90°$) site, the FCC ($\vartheta = 90°$, $\varphi = 330°$) site, and the t2f ($\vartheta = 90°$, $\varphi = 240°$) site.

	Top (early)	(late)	Bridge	FCC	t2f (early)	(late)
PBEα-vdW-DF	–	−34	−18	22	−115	−65
PBE	−5	0	83	118	12	−75
PBE-vdW-DF	−93	158	116	157	−6	133
RPBE	66	307	276	322	165	227

for the four PESs obtained with the different XC functionals. The first thing to note is that, as expected, the barrier heights are highly dependent on the choice of XC functional. The variation of the barrier height with impact site is also heavily dependent on the XC functional. For example for PBE the bridge site has a higher barrier than the top site, but for PBE-vdW-DF the barrier of the bridge site is actually lower than that of the top site.

The barrier heights and positions for the dissociation of H_2 on Pd(111) can be found in figure 5.4. Here, the top-to-bridge (top $\vartheta = 90°$, $\varphi = 0°$) cut of the potential energy is shown and the location of the barriers for the other configurations used in the construction of the PES are shown by the closed (early barriers) and open (late barriers) symbols. The colour of these symbols indicate the barrier height, with red symbols indicating energetically low barriers, and blue symbols indicating energetically high barriers. It can be seen from the figure that there is a correlation between barrier height and barrier position. The general trend is that late barriers are energetically higher than early barriers. It should be noted that, especially for PBE, this trend can be divided into two separate regimes, *i.e.*, $r < 1$ Å, and $r > 1$ Å.

The interpolation of the PESs by the CRP has been tested thoroughly. QCT calculations were used to sample configurations of the PES which are dynamically relevant. For each PES, all the intermediate points of 100 trajectories were logged for the seven different nozzle temperatures of the calculated molecular beams (see table 5.1). For 500 points

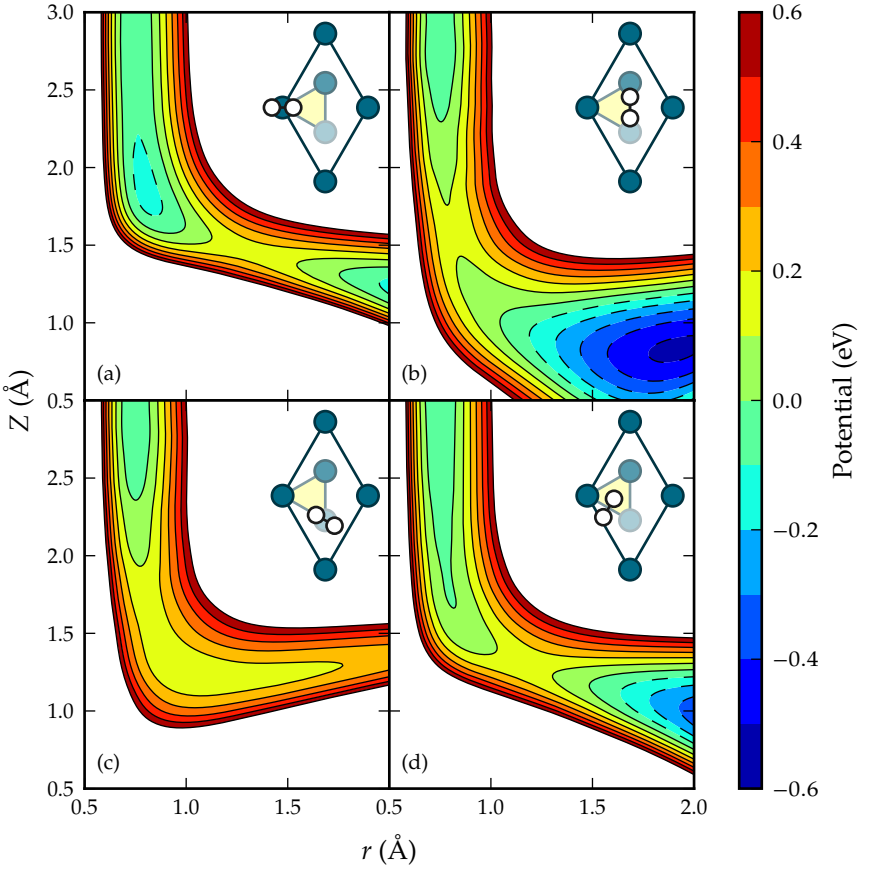

Figure 5.3 2D contour plots (in Z and r) of the PBE-vdW-DF PES for four different configurations. The configurations are the (a) top ($\vartheta = 90°$, $\varphi = 0°$), (b) bridge ($\vartheta = 90°$, $\varphi = 90°$), (c) FCC ($\vartheta = 90°$, $\varphi = 330°$), and (d) t2f ($\vartheta = 90°$, $\varphi = 240°$) dissociation geometries. The zero of the potential energy is set to the gas-phase minimum energy, and the contours span the interval [−0.6, 0.6] eV, with steps of 100 meV.

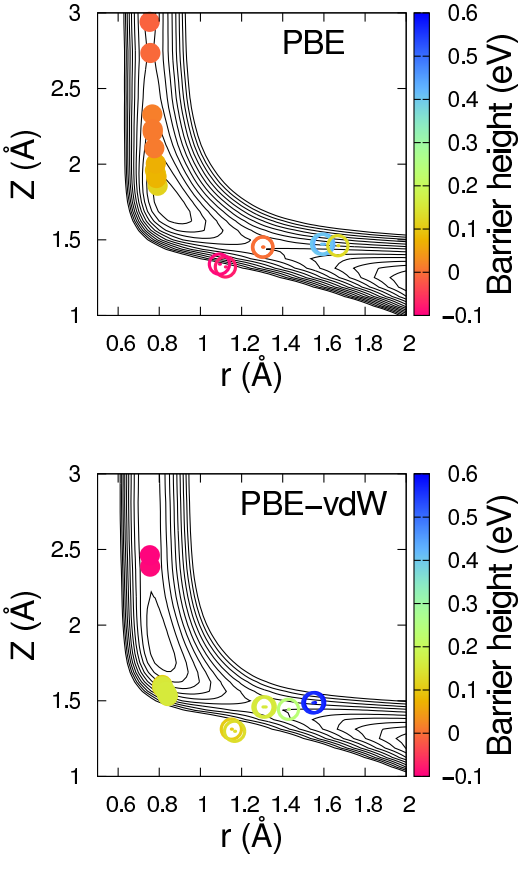

Figure 5.4 Barrier heights and positions for H_2 on Pd(111) for the computed configurations used in the construction of the PES, together with the top-to-bridge (top $\vartheta = 90°$, $\varphi = 0°$) cut of the PES. Closed symbols denote early barriers, and open symbols denote late barriers. The zero of the potential energy is set equal to the gas-phase minimum energy, and the solid line contours span the interval $[-1, 0.35]$ eV, with steps of 50 meV.

(which were randomly extracted) per PES, the quality of interpolation was tested. Those points were binned on their respective Z value in order to test the PES for specific regions. Bin 1 has Z values of 4 to 6.5 Å, which corresponds to the gas-phase. The early barrier region has Z values between 2 and 4 Å, which are binned in bin 2. All the points, which have Z values of less than 2 Å, were additionally binned on their r value. Bin 3 has r values which are smaller than 1.5 Å, these correspond to the late barrier region. Finally, bin 4 has the points where $r > 1.5$ Å; the points in this bin correspond to trajectories which have already reacted, and these points are therefore dynamically the least important. The results, which can be found in table 5.5, show that the root mean square error (RMSE) is small for the gas-phase and early barrier region ($\sim$ 1 to 5 meV), and somewhat larger for the late barrier region (roughly $12 - 17$ meV). The largest absolute error which can be found for each PES, however, is on the order of 50 to 100 meV, and can be found in the late barrier region (bin 3). From this it can be concluded that, although overall the CRP works quite well, for specific cases the error in the interpolation of the PES can be rather large. The RMSE values reported here are somewhat larger than in previous studies,[6,71] because of the used testing procedure. Here, the sampled points were selected at random from dynamics calculations, which is more thorough than previous tests where potential cuts in only one or two dimensions were considered.

5.3.2 Molecular beam sticking probabilities

The accuracy of the reaction probabilities obtained with classical and QCT methods for H_2/Pd(111) has been studied extensively.[21,24,26] It was found that for this system the QCT method describes dynamic trapping poorly, because dynamic trapping is quenched due to an unphysical conversion of vibrational ZPE to rotational energy. The classical trajectory (CT) method describes the role of dynamic trapping much better because no initial ZPE is present. Direct dissociation, however, is not well described by the CT method. The result is that at low incidence energies both of the methods are not able to accurately calculate the reaction probability. For high incidence energies the QCT method is,

Table 5.5 RMSE for all four different computed PESs. The test points are sampled from QCT calculations and are randomly extracted. All the test points are binned according to their Z value. For $Z < 2$ Å the test points are additionally binned according to their r value.

	Bin 1 $Z = 4 - 6.5$ Å all r values		Bin 2 $Z = 2 - 4$ Å all r values		Bin 3 $Z = 0 - 2$ Å $r \leq 1.5$ Å		Bin 4 $Z = 0 - 2$ Å $r > 1.5$ Å	
PES	N	RMSE (meV)	N	RMSE (meV)	N	RMSE (meV)	N	RMSE (meV)
PBE	174	1.0	218	3.1	85	16.9	23	27.4
PBE-vdW-DF	153	2.9	307	5.5	36	12.2	4	22.9
RPBE	213	0.8	246	4.9	34	13.2	7	29.7
PBEα-vdW-DF	143	3.1	243	3.9	86	13.6	28	20.4

CHAPTER 5

Towards a specific reaction parameter density functional for reactive scattering of H_2 from Pd(111)

however, in good agreement with QD, because dynamic trapping does not play a significant role for high incidence energies.[24]

Therefore, in order to check the performance of XC functionals it is best to compare reaction probabilities obtained with the QCT method with experiments for high incidence energies. If a good candidate SRP functional is found, QD calculations can then be performed for this XC functional. The results of QD calculations can then be compared with experimental sticking probabilities over the entire incidence energy region to assess the quality of the functional.

In figure 5.5, the experimental sticking probability of the latest (and presumably best) molecular beam experiment from the Rendulic group[16,17] is compared with the simulated molecular beam reaction probabilities obtained with the QCT method for four different PESs for the incidence energy region of $125 - 400$ meV, for which the QCT method should work reasonably well. It can be seen that the probability of hydrogen dissociation on Pd(111) is heavily dependent on the choice of the XC functional used in the DFT calculation of the PES. Furthermore, the reaction probability obtained with the PBE-vdW-DF functional is in reasonable agreement with experiment. Therefore, out of these functionals, the PBE-vdW-DF XC functional seems the best candidate. Hence, QD calculations will be performed for this functional only.

In order to validate if the candidate functional is indeed able to describe the molecular beam experiment also for low energies, QD calculations were performed for the PBE-vdW-DF functional. In figure 5.6, the experimental molecular beam sticking probabilities are presented from Gostein and Sitz[18] (labeled exp. Sitz), and from Lesnik[16] and Beutl *et al.*[17] (labeled exp. Rendulic 2001). The reaction probabilities obtained with the PBE-vdW-DF functional computed with the QCT method and with QD can also be found in this figure. Unfortunately, the molecular beam simulations using QD are not able to reproduce the non-monotonic behaviour of the experiment. Therefore, assuming the BOSS model gives correct results, we can disregard the PBE-vdW-DF functional as a good candidate for the specific reaction parameter functional for H_2/Pd(111). In fact, the QD molecular beam result is not a significant improvement over the molecular beam results obtained

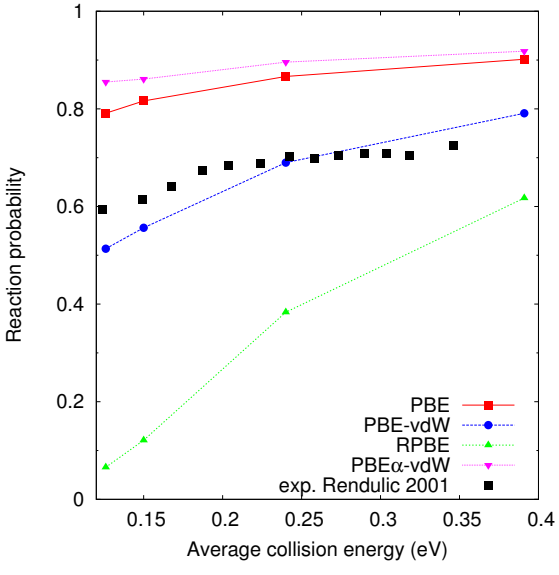

Figure 5.5 Reaction probabilities of the simulated molecular beams computed with the QCT method alongside the experimental molecular beam sticking probabilities performed by Lesnik[16] and Beutl *et al.*[17] (labeled exp. Rendulic 2001) for an incidence energy interval of 125 − 400 meV.

with the QCT method. This suggests that (for the selected functional) quantum effects, such as ZPE and tunnelling do not play an important role, and that most of the reaction occurs classically over the energy barrier. The lack of dynamic trapping could therefore be due to the PES rather than to the use of the QCT method. It is however important to note that dynamic trapping can also be enhanced by allowing energy exchange with surface atoms,[27,28] which suggests that, apart from the functional, also surface temperature effects may need to be taken into account.

Note that the point at 35 meV (corresponding to $T_n = 100$ K) is omitted for the PBE-vdW-DF QD results. This was done because there is a large uncertainty for that point, which arises from the extrapolation of the state-resolved reaction curves towards low incidence energies. For Pd(111) it is non-trivial how to extrapolate towards low incidence energies. For activated systems the reaction curve can be extrapolated to

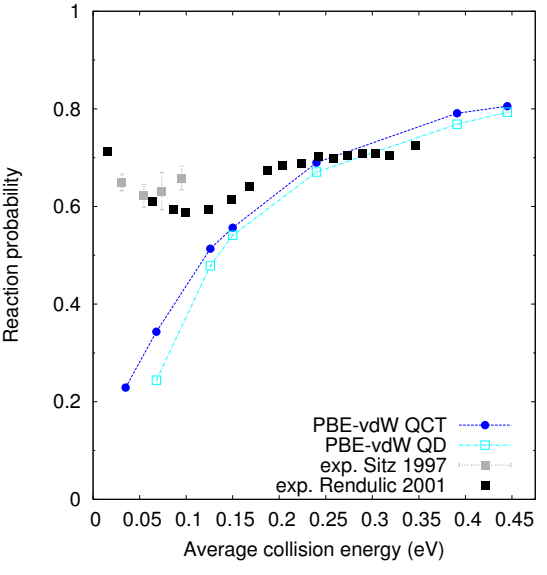

Figure 5.6 Reaction probabilities obtained with the PBE-vdW-DF functional for the simulated molecular beams computed with the QCT method, and with QD are compared with the most experimental molecular beam sticking probabilities. The experiment by Gostein and Sitz[18] is labelled exp. Sitz 1997, and the experiment performed by Lesnik[16] and Beutl *et al.*[17] is labelled exp. Rendulic 2001.

zero, but for this non-activated system it is not clear how to extrapolate towards low incidence energies. Tests with several extrapolation schemes indicated that the resulting uncertainty in the reaction probability in the point at 35 meV can be as large as 30%. Fortunately, for all other calculated points this extrapolation towards low incidence energies does not significantly change the reaction probability (changes are in the order of 0.001).

5.3.3 Initial state-resolved reaction probabilities

The discrepancy between the molecular beam experiment and the simulated molecular beam with QD can have multiple causes: (i) effects of surface motion are not modelled, because of the static surface approximation in the BOSS method;[10] (ii) incorrect assumptions about the dis-

tribution of energies in the molecular beam can introduce errors; and (iii) errors in the anisotropy and corrugation of the PES. In this work, it is not studied whether surface motion plays an important role in the dissociation of H_2 on Pd(111), which may be important for properly describing trapping of molecules, and trapping mediated reaction.[27,28] In order to clarify the latter two points the initial state-resolved (degeneracy averaged) reaction probabilities obtained with the QCT method using four different PESs, and reaction probabilities obtained with QD for PBE-vdW-DF will be compared with the state-resolved experiment by Gostein and Sitz.[18]

In figure 5.7, initial state-resolved (degeneracy averaged) reaction probabilities can be found for the ($v = 0, J = 0$) and ($v = 0, J = 1$) states. Again, as expected, the state-resolved reaction probabilities are very dependent on the choice of XC functional. The PBE-vdW-DF functional clearly underestimates the initial state-resolved reaction probabilities for the ($v = 0, J = 0$) and ($v = 0, J = 1$) states. There is a good agreement between the state-resolved reaction probabilities obtained with the QCT method and those obtained with QD for the PBE-vdW-DF functional, especially for the ($v = 0, J = 1$) state. This confirms the previous conclusion that quantum effects do not play an important role in the reaction probability for this functional. The discrepancy observed for low incidence energies between the simulated molecular beams and the molecular beam experiments are probably not only caused by errors in the distribution of energies in the molecular beam, because also for the initial state-resolved reaction probabilities there is a discrepancy between experiment and the calculations. Furthermore, for low translational energies the width of the translational energy distribution in experiments tends to be narrow.

Surprisingly, for the ($v = 0, J = 0$) state, there is an excellent agreement between the calculated reaction probability obtained for the PBEα-vdW-DF functional and the state-resolved experiment by Gostein and Sitz.[18] For the reaction probability of the ($v = 0, J = 1$) state, however, this good agreement is not reproduced, as can be seen on the right panel of figure 5.7. Here, PBEα-vdW-DF clearly overestimates the reaction probability for dissociation of hydrogen on Pd(111).

In order to elucidate the origin of the discrepancy between calcu-

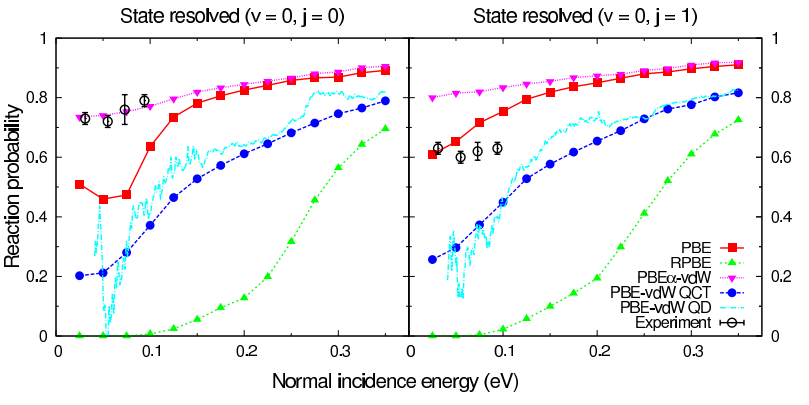

Figure 5.7 Rotational state-resolved reaction probabilities of the dissociation of hydrogen on a Pd(111) surface. On the left ($v = 0$, $J = 0$), and on the right ($v = 0$, $J = 1$). The experiment[18] was performed with a surface temperature of 423 K. If not mentioned otherwise the calculated results are obtained with the QCT method. The quantum results have been smoothed by a weighted Gaussian with a width of 0.5 meV.

lated reaction probabilities and experiment, the reaction probability of H_2 dissociating on a Pd(111) surface has been plotted versus the initial rotational state (J) for an incidence energy of 94 meV. This is shown in figure 5.8. For all functionals the reaction probability increases with J up to $J = 2$ for the calculations performed with the QCT method. Then, for all functionals except RPBE, the reaction probability decreases with increasing J and stabilizes. Experimentally, however, a sharp decrease in reaction probability is observed between $J = 0$ and $J = 1$.[18] After that, the reaction probability increases a little and stabilizes. The QD calculations show a small improvement over the QCT calculations, but they are also not able to reproduce the experimental trend in the dependence of the reaction probability on J. The calculations cannot reproduce the decrease in reaction probability with increasing rotational quantum number (J), as is experimentally found.

5.3.4 Comparison to experiment and outlook

The discrepancies noted between the experiments and the theoretical calculations on H_2/Pd(111) can be due to several reasons, *i.e.*, (i) errors

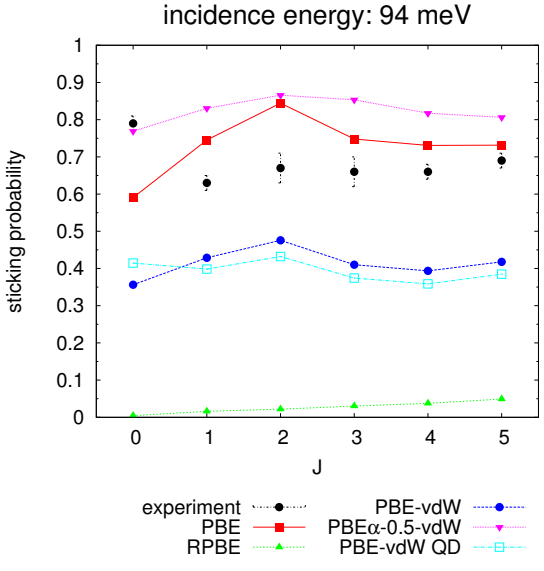

Figure 5.8 Dissociative reaction probability as a function of initial quantum number J for an incidence energy of 94 meV. If not mentioned otherwise the calculated results are obtained with the QCT method. The state-resolved experiments were performed by Gostein and Sitz.[18]

in the experiments; (ii) errors in the simulation of the experiments due to assuming wrong translational energy distributions or nozzle temperatures; (iii) errors in the PES used; and (iv) errors in the dynamical model used. These error sources will now be discussed one by one, ending with a brief outlook on how progress may be achieved with modelling the reactive scattering of H_2 from Pd(111) in future work.

As noted already in the introduction rather diverse sets of measurements have been published on sticking of H_2 on Pd(111). The latest set of measurements from the Rendulic group[16,17] and the measurements by Gostein and Sitz[18] are in reasonable agreement with one another, but they still differ from one another at the higher incidence energies probed by Gostein and Sitz (see figure 5.1). Also, for neither set of measurements the beam conditions have been published, while accurate calculations on H_2/Cu(111)[6] show that the knowledge of the nozzle temperature and the parameters characterising the translational energy

distribution of H_2 beams is essential for accurately simulating reactive scattering of H_2 from metal surfaces. The absence of these data (the assumption had to be made that the beam parameters for H_2/Pd(111) were the same as those used in other experiments of the Rendulic group on H_2/Cu(111)) makes it harder to describe the experiments on these systems accurately. The result that the sticking probability first decreases and then increases with incidence energy is, however, not in doubt, as it is observed in all the measurements shown in figure 5.1. We also note that knowledge of the translational energy distributions is less critical to simulating sticking measurements for low average incidence energies, as the translational energy distributions are typically rather narrow for low incidence energies (nozzle temperatures).

Errors in the PES can be due to errors in the interpolation of the DFT data and to the density functional yielding an inaccurate description of the molecule–surface interaction. Due to the accuracy of the CRP method used to interpolate the PES for H_2/Pd(111) (see section 5.3.1) and other H_2 + metal surface systems (see for instance references 6 and 44) it can be safely assumed that if errors in the PES are to blame for the discrepancy with experiment, then they are most likely due to the use of an inaccurate density functional. This point will now be discussed in more detail.

The discrepancies of the dynamics results based on the PBE-vdW-DF candidate SRP density functional with the measured sticking probabilities and initial state-resolved reaction probabilities can be summarized as follows. (i) Although the computed sticking probabilities are in reasonable agreement with the experiments of Lesnik[16] and Beutl *et al.*[17] for incidence energies ≥ 125 meV, the computed reaction probability curve does not show the upturn occurring at low energies with decreasing incidence energy, as manifest in both the experiments of Lesnik[16] and Beutl *et al.*[17] and those by Gostein and Sitz.[18] (ii) The computed initial state-resolved reaction probabilities do not show the decrease occurring in the experimental results going from non-rotating H_2 ($J = 0$) to rotating H_2 ($J = 1 - 5$). Both experimental observations are manifestations of a reaction mechanism whereby the molecule reacts without barrier either through "steering"[36,37] or "dynamic trapping".[25,26] Molecules with a low incidence energy are more easily

trapped at the surface through energy transfer from translation to rotation,[25] and have more time to be steered to sites or orientations for which reaction is barrierless.[36] Likewise, non-rotating molecules are more easily steered to an orientation for which reaction is barrierless,[37] and they are more easily dynamically trapped.[26] Both discrepancies with experiment therefore point to one and the same defect in the theoretical treatment: the correct functional should show barrierless dissociation for at least some impact sites and orientations. The problem with the candidate PBE-vdW-DF SRP density functional is that it does not show barrierless dissociation for any of the high symmetry sites investigated. The fact that it performs well for high incidence energies suggests that a functional is needed with a broader distribution of barrier heights over the impact sites, with the distribution of barrier heights skewed more to lower energies than obtained for the PBE-vdW-DF density functional.

Finally, the discrepancies between theory and experiment can in principle also de due to the dynamical model (the BOSS model) being inadequate to describe the experiments on H_2/Pd(111) here discussed. For reasons discussed in section 5.2.1, it is it unlikely that the Born–Oppenheimer approximation is responsible for the large deviations between experiment and theory. The presence of phonons in the dynamical model might facilitate trapping, but for this to facilitate reaction at low incidence energies a PES which shows barrierless dissociation for at least some impact sites and orientations would still be needed. In previous calculations on this system, energy exchange was found to alter the probability for trapping.[27,28] The PES used in these studies however already showed barrierless dissociation if energy exchange was not taken into account. For these reasons, the dynamical model is not the first place to look for improvements of the theoretical description of the reactive scattering experiments on H_2/Pd(111) discussed here, but the possibility that phonons are needed for an accurate description of these experiments cannot be excluded.

It is therefore suggested that future theoretical calculations on H_2/Pd(111) first investigate the performance of candidate SRP density functionals which have a broader distribution of barrier heights for this system, so that they show barrierless dissociation for at least some impact sites and orientations, while showing similar barrier heights

at the high energy end of the spectrum. The availability of new well-characterised molecular beam sticking experiments on H_2/Pd(111) (or detailed information on the beam parameters used in the experiments of Lesnik *et al.* and of Gostein and Sitz) would also facilitate the development of an accurate theoretical description of this system. The availability of new and well-characterised molecular beam sticking experiments on H_2/Pd(100) would also be useful, as associative desorption experiments are also available for this system,[34,78] and an SRP density functional developed for H_2 interacting with the Pd(100) surface is likely to be accurate for H_2/Pd(111) as well.[13]

5.4 Summary and conclusions

Potential energy surfaces have been calculated for H_2/Pd(111) for four different XC functionals. The barrier heights are highly dependent on the choice of XC functional. Moreover, the way in which the barrier height varies with the impact site is also dependent on the choice of XC functional. It is found that there is a correlation between the barrier height and barrier position, where the general trend is that late barriers are energetically higher than early barriers. With the CRP method used to interpolate the DFT results, the RMSE of the interpolation of the PESs is small for the gas-phase and early barrier region ($\sim$ 1 to 5 meV), and somewhat larger for the late barrier region (roughly 12 to 17 meV).

A candidate SRP density functional was obtained by comparing simulated molecular beam reaction probabilities obtained with the QCT method with experimental sticking probabilities for high incidence energy (above 125 meV). The reaction probability is, as expected, heavily dependent on the choice of XC functional. The PBE-vdW-DF functional was proposed as a candidate XC functional describing the reactive scattering of H_2 on Pd(111), because at high incidence energies simulated molecular beam reaction probabilities obtained with the QCT method were in reasonable agreement with experimental sticking probabilities. In order to check the validity of the candidate functional, QD calculations were performed for the PBE-vdW-DF functional. The simulated molecular beam results obtained with QD, however, were not in good agreement with experimental sticking probabilities at low incidence en-

ergies. Therefore, the candidate (PBE-vdW-DF) XC functional is disregarded. The fact that the QD molecular beam simulated results are not a significant improvement over the QCT results suggest that (for the selected functional) quantum effects, such as ZPE conservation and tunnelling, do not play an important role in the reactive scattering of H_2 on Pd(111). In previous calculations,[24] steering effects were observed in the QD calculation of H_2 on Pd(111), with the PES of Dong and Hafner[20] and Busnengo *et al.*[25] based on the PW91 functional.[79]

Among the possible origins of the discrepancies between the theoretical PBE-vdW-DF results and the experimental results for H_2/Pd(111), the most likely cause is that the functional used does not yield barrierless dissociation for at least some impact sites and orientations, so that the upturn of the reaction probability curve at low incidence energy is not recovered. It is therefore suggested that the use of a density functional yielding a broader barrier height distribution (and barrierless dissociation for at least some impact sites and orientations) is explored first to achieve a more accurate theoretical description of H_2 on Pd(111). For this, the availability of new well-characterised molecular beam sticking experiments on H_2/Pd(111) or Pd(100) (or detailed information on the beam parameters used in the experiments of Lesnik and of Gostein and Sitz on H_2/Pd(111)) would also be helpful. Additionally surface temperature effects should be taken into account, as this may provide an increased probability for trapping.[27,28]

References

[1] C. T. Rettner, D. J. Auerbach, J. C. Tully, and A. W. Kleyn. Chemical dynamics at the gas-surface interface. *Journal of Physical Chemistry* **100**(31), pp. 13021–13033, 1996.

[2] V. Smil. Detonator of the population explosion. *Nature* **400**(6743), p. 415, 1999.

[3] G. A. Somorjai and Y. Li. Impact of surface chemistry. *Proceedings of the National Academy of Sciences* **108**(3), pp. 917–924, 2011.

[4] K. Honkala, A. Hellman, I. N. Remediakis, A. Logadottir, A. Carlsson, S. Dahl, C. H. Christensen, and J. K. Nørskov. Ammonia synthesis from first-principles calculations. *Science* **307**(5709), pp. 555–558, 2005.

[5] G. J. Kroes. Frontiers in surface scattering simulations. *Science* **321**(5890), pp. 794–797, 2008.

[6] C. Díaz, E. Pijper, R. A. Olsen, H. F. Busnengo, D. J. Auerbach, and G. J. Kroes. Chemically accurate simulation of a prototypical surface reaction: H_2 dissociation on Cu(111). *Science* **326**(5954), pp. 832–834, 2009.

[7] B. Hammer, M. Scheffler, K. W. Jacobsen, and J. K. Nørskov. Multidimensional potential energy surface for H_2 dissociation over Cu(111). *Physical Review Letters* **73**(10), pp. 1400–1403, 1994.

[8] J. Zheng, Y. Zhao, and D. G. Truhlar. The DBH24/08 database and its use to assess electronic structure model chemistries for chemical reaction barrier heights. *Journal of Chemical Theory and Computation* **5**(4), pp. 808–821, 2009.

[9] K. Yang, J. Zheng, Y. Zhao, and D. G. Truhlar. Tests of the RPBE, revPBE, τ-HCTHhyb, ωB97X-D, and MOHLYP density functional approximations and 29 others against representative databases for diverse bond energies and barrier heights in catalysis. *Journal of Chemical Physics* **132**(16), 164117, 2010.

[10] G. J. Kroes and C. Díaz. Quantum and classical dynamics of reactive scattering of H_2 from metal surfaces. Accepted to *Chemical Society Reviews*. doi: 10.1039/C5CS00336A. 2016.

[11] Y. Y. Chuang, M. L. Radhakrishnan, P. L. Fast, C. J. Cramer, and D. G. Truhlar. Direct dynamics for free radical kinetics in solution: solvent effect on the rate constant for the reaction of methanol with atomic hydrogen. *Journal of Physical Chemistry A* **103**(25), pp. 4893–4909, 1999.

[12] A. Chakraborty, Y. Zhao, H. Lin, and D. G. Truhlar. Combined valence bond-molecular mechanics potential-energy surface and direct dynamics study of rate constants and kinetic isotope effects for the H + C_2H_6 reaction. *Journal of Chemical Physics* **124**(4), 044315, 2006.

[13] L. Sementa, M. Wijzenbroek, B. J. van Kolck, M. F. Somers, A. Al-Halabi, H. F. Busnengo, R. A. Olsen, G. J. Kroes, M. Rutkowski, C. Thewes, N. F. Kleimeier, and H. Zacharias. Reactive scattering of H_2 from Cu(100): comparison of dynamics calculations based on the specific reaction parameter approach to density functional theory with experiment. *Journal of Chemical Physics* **138**(4), 044708, 2013.

[14] Ch. Resch, H. F. Berger, K. D. Rendulic, and E. Bertel. Adsorption dynamics for the system hydrogen/palladium and its relation to the surface electronic structure. *Surface Science* **316**(3), pp. L1105–L1109, 1994.

[15] M. Beutl, M. Riedler, and K. D. Rendulic. Strong rotational effects in the adsorption dynamics of H_2/Pd(111): evidence for dynamical steering. *Chemical Physics Letters* **247**(3), pp. 249–252, 1995.

[16] J. Lesnik. Untersuchungen über Vorläuferadsorption an Übergangsmetallen und Übergangsmetallegierungen. PhD thesis. Technischen Universität Graz, 2001.

[17] M. Beutl, J. Lesnik, K. D. Rendulic, R. Hirschl, A. Eichler, G. Kresse, and J. Hafner. There is a true precursor for hydrogen adsorption after all: the system H_2/Pd(111) + subsurface V. *Chemical Physics Letters* **342**(5–6), pp. 473–478, 2001.

[18] M. Gostein and G. O. Sitz. Rotational state-resolved sticking coefficients for H_2 on Pd(111): testing dynamical steering in dissociative adsorption. *Journal of Chemical Physics* **106**(17), pp. 7378–7390, 1997.

[19] A. Winkler. Personal communication. 2012.

[20] W. Dong and J. Hafner. H_2 dissociative adsorption on Pd(111). *Physical Review B* **56**(23), pp. 15396–15403, 1997.

[21] H. F. Busnengo, A. Salin, and W. Dong. Representation of the 6D potential energy surface for a diatomic molecule near a solid surface. *Journal of Chemical Physics* **112**(17), pp. 7641–7651, 2000.

[22] C. Crespos, H. F. Busnengo, W. Dong, and A. Salin. Analysis of H_2 dissociation dynamics on the Pd(111) surface. *Journal of Chemical Physics* **114**(24), pp. 10954–10962, 2001.

[23] H. F. Busnengo, C. Crespos, W. Dong, A. Salin, and J. C. Rayez. Role of orientational forces in nonactivated molecular dissociation on a metal surface. *Physical Review B* **63**(4), 041402, 2001.

[24] H. F. Busnengo, E. Pijper, M. F. Somers, G. J. Kroes, A. Salin, R. A. Olsen, D. Lemoine, and W. Dong. Six-dimensional quantum and classical dynamics study of H_2(v=0,J=0) scattering from Pd(111). *Chemical Physics Letters* **356**(5–6), pp. 515–522, 2002.

[25] H. F. Busnengo, C. Crespos, W. Dong, J. C. Rayez, and A. Salin. Classical dynamics of dissociative adsorption for a nonactivated system: the role of zero point energy. *Journal of Chemical Physics* **116**(20), pp. 9005–9013, 2002.

[26] H. F. Busnengo, E. Pijper, G. J. Kroes, and A. Salin. Rotational effects in dissociation of H_2 on Pd(111): quantum and classical study. *Journal of Chemical Physics* **119**(23), pp. 12553–12562, 2003.

[27] H. F. Busnengo, W. Dong, and A. Salin. Trapping, molecular adsorption, and precursors for nonactivated chemisorption. *Physical Review Letters* **93**(23), 236103, 2004.

[28] H. F. Busnengo, M. A. Di Césare, W. Dong, and A. Salin. Surface temperature effects in dynamic trapping mediated adsorption of light molecules on metal surfaces: H_2 on Pd(111) and Pd(110). *Physical Review B* **72**(12), 125411, 2005.

[29] H. F. Busnengo, W. Dong, P. Sautet, and A. Salin. Surface temperature dependence of rotational excitation of H_2 scattered from Pd(111). *Physical Review Letters* **87**(12), 127601, 2001.

[30] C. Díaz, H. F. Busnengo, F. Martin, and A. Salin. Angular distribution of H_2 molecules scattered from the Pd(111) surface. *Journal of Chemical Physics* **118**(6), pp. 2886–2892, 2003.

[31] K. D. Rendulic, G. Anger, and A. Winkler. Wide range nozzle beam adsorption data for the systems H_2/nickel and H_2/Pd(100). *Surface Science* **208**(3), pp. 404–424, 1989.

[32] C. T. Rettner and D. J. Auerbach. Search for oscillations in the translational energy dependence of the dissociation of H_2 on Pd(100). *Chemical Physics Letters* **253**(3–4), pp. 236–240, 1996.

[33] D. Wetzig, R. Dopheide, M. Rutkowski, R. David, and H. Zacharias. Rotational alignment in associative desorption of $D_2(v'' = 0$ and 1) from Pd(100). *Physical Review Letters* **76**(3), pp. 463–466, 1996.

[34] D. Wetzig, M. Rutkowski, W. Etterich, R. David, and H. Zacharias. Rotational alignment in associative desorption of H_2 from Pd(100). *Surface Science* **402–404**, pp. 232–235, 1998.

[35] D. Barredo, G. Laurent, C. Díaz, P. Nieto, H. F. Busnengo, A. Salin, D. Farías, and F. Martín. Experimental evidence of dynamic trapping in the scattering of H_2 from Pd(110). *Journal of Chemical Physics* **125**(5), 051101, 2006.

[36] A. Gross, S. Wilke, and M. Scheffler. Six-dimensional quantum dynamics of adsorption and desorption of H_2 at Pd(100): steering and steric effects. *Physical Review Letters* **75**(14), pp. 2718–2721, 1995.

[37] A. Gross, S. Wilke, and M. Scheffler. Six-dimensional quantum dynamics of adsorption and desorption of H_2 at Pd(100): no need for a molecular precursor adsorption state. *Surface Science* **357–358**, pp. 614–618, 1996.

[38] A. Gross and M. Scheffler. *Ab initio* quantum and molecular dynamics of the dissociative adsorption of hydrogen on Pd(100). *Physical Review B* **57**(4), pp. 2493–2506, 1998.

[39] A. Gross. *Ab initio* molecular dynamics simulations of the adsorption of H_2 on palladium surfaces. *ChemPhysChem* **11**(7), pp. 1374–1381, 2010.

[40] A. Gross. Coverage effects in the adsorption of H_2 on Pd(100) studied by *ab initio* molecular dynamics simulations. *Journal of Chemical Physics* **135**(17), 174707, 2011.

[41] M. A. Di Césare, H. F. Busnengo, W. Dong, and A. Salin. Role of dynamic trapping in H_2 dissociation and reflection on Pd surfaces. *Journal of Chemical Physics* **118**(24), pp. 11226–11234, 2003.

[42] A. Dianat and A. Gross. High-dimensional quantum dynamical study of the dissociation of H_2 on Pd(110). *Journal of Chemical Physics* **120**(11), pp. 5339–5346, 2004.

[43] C. Díaz, F. Martín, H. F. Busnengo, and A. Salin. Theoretical analysis of the relation between H_2 dissociation and reflection on Pd surfaces. *Journal of Chemical Physics* **120**(1), pp. 321–328, 2004.

[44] P. Nieto, E. Pijper, D. Barredo, G. Laurent, R. A. Olsen, E. J. Baerends, G. J. Kroes, and D. Farías. Reactive and nonreactive scattering of H_2 from a metal surface is electronically adiabatic. *Science* **312**(5770), pp. 86–89, 2006.

[45] A. C. Luntz and M. Persson. How adiabatic is activated adsorption/associative desorption? *Journal of Chemical Physics* **123**(7), 074704, 2005.

[46] J. I. Juaristi, M. Alducin, R. Díez Muiño, H. F. Busnengo, and A. Salin. Role of electron–hole pair excitations in the dissociative adsorption of diatomic molecules on metal surfaces. *Physical Review Letters* **100**(11), 116102, 2008.

[47] G. Füchsel, S. Schimka, and P. Saalfrank. On the role of electronic friction for dissociative adsorption and scattering of hydrogen molecules at a Ru(0001) surface. *Journal of Physical Chemistry A* **117**(36), pp. 8761–8769, 2013.

[48] C. Díaz, R. A. Olsen, D. J. Auerbach, and G. J. Kroes. Six-dimensional dynamics study of reactive and non reactive scattering of H_2 from Cu(111) using a chemically accurate potential energy surface. *Physical Chemistry Chemical Physics* **12**(24), pp. 6499–6519, 2010.

[49] F. Nattino, C. Díaz, B. Jackson, and G. J. Kroes. Effect of surface motion on the rotational quadrupole alignment parameter of D_2 reacting on Cu(111). *Physical Review Letters* **108**(23), 236104, 2012.

[50] A. Mondal, M. Wijzenbroek, M. Bonfanti, C. Díaz, and G. J. Kroes. Thermal lattice expansion effect on reactive scattering of H_2 from Cu(111) at T_s = 925 K. *Journal of Physical Chemistry A* **117**(36), pp. 8770–8781, 2013.

[51] G. Kresse and J. Hafner. *Ab initio* molecular dynamics for liquid metals. *Physical Review B* **47**(1), pp. 558–561, 1993.

[52] G. Kresse and J. Hafner. *Ab initio* molecular-dynamics simulation of the liquid-metal–amorphous-semiconductor transition in germanium. *Physical Review B* **49**(20), pp. 14251–14269, 1994.

[53] G. Kresse and J. Furthmüller. Efficiency of *ab initio* total energy calculations for metals and semiconductors using a plane-wave basis set. *Computational Materials Science* **6**(1), pp. 15–50, 1996.

[54] G. Kresse and J. Furthmüller. Efficient iterative schemes for *ab initio* total-energy calculations using a plane-wave basis set. *Physical Review B* **54**(16), pp. 11169–11186, 1996.

[55] G. te Velde and E. J. Baerends. Precise density-functional method for periodic structures. *Physical Review B* **44**(15), pp. 7888–7903, 1991.

[56] G. te Velde and E. J. Baerends. Slab versus cluster approach for chemisorption studies. CO on Cu(100). *Chemical Physics* **177**(2), pp. 399–406, 1993.

[57] R. A. Olsen, G. J. Kroes, and E. J. Baerends. Atomic and molecular hydrogen interacting with Pt(111). *Journal of Chemical Physics* **111**(24), pp. 11155–11163, 1999.

[58] T. J. Frankcombe, M. A. Collins, and D. H. Zhang. Modified Shepard interpolation of gas-surface potential energy surfaces with strict plane group symmetry and translational periodicity. *Journal of Chemical Physics* **137**(14), 144701, 2012.

[59] J. P. Perdew, K. Burke, and M. Ernzerhof. Generalized gradient approximation made simple. *Physical Review Letters* **77**(18), pp. 3865–3868, 1996.

[60] B. Hammer, L. B. Hansen, and J. K. Nørskov. Improved adsorption energetics within density-functional theory using revised Perdew-Burke-Ernzerhof functionals. *Physical Review B* **59**(11), pp. 7413–7421, 1999.

[61] M. Dion, H. Rydberg, E. Schröder, D. C. Langreth, and B. I. Lundqvist. Van der Waals density functional for general geometries. *Physical Review Letters* **92**(24), 246401, 2004.

[62] G. K. H. Madsen. Functional form of the generalized gradient approximation for exchange: the PBEα functional. *Physical Review B* **75**(19), 195108, 2007.

[63] J. Klimeš, D. R. Bowler, and A. Michaelides. Van der Waals density functionals applied to solids. *Physical Review B* **83**(19), 195131, 2011.

[64] G. Román-Pérez and J. M. Soler. Efficient implementation of a van der Waals density functional: application to double-wall carbon nanotubes. *Physical Review Letters* **103**(9), 096102, 2009.

[65] M. A. L. Marques, M. J. T. Oliveira, and T. Burnus. Libxc: a library of exchange and correlation functionals for density functional theory. *Computer Physics Communications* **183**(10), pp. 2272–2281, 2012.

[66] P. E. Blöchl. Projector augmented-wave method. *Physical Review B* **50**(24), pp. 17953–17979, 1994.

[67] G. Kresse and D. Joubert. From ultrasoft pseudopotentials to the projector augmented-wave method. *Physical Review B* **59**(3), pp. 1758–1775, 1999.

[68] D. Vanderbilt. Soft self-consistent pseudopotentials in a generalized eigenvalue formalism. *Physical Review B* **41**(11), pp. 7892–7895, 1990.

[69] G. Kresse and J. Hafner. Norm-conserving and ultrasoft pseudopotentials for first-row and transition elements. *Journal of Physics: Condensed Matter* **6**(40), pp. 8245–8257, 1994.

[70] E. Pijper, G. J. Kroes, R. A. Olsen, and E. J. Baerends. The effect of corrugation on the quantum dynamics of dissociative and diffractive scattering of H_2 from Pt(111). *Journal of Chemical Physics* **113**(18), pp. 8300–8312, 2000.

[71] R. A. Olsen, H. F. Busnengo, A. Salin, M. F. Somers, G. J. Kroes, and E. J. Baerends. Constructing accurate potential energy surfaces for a diatomic molecule interacting with a solid surface: H_2+Pt(111) and H_2+Cu(100). *Journal of Chemical Physics* **116**(9), pp. 3841–3855, 2002.

[72] R. Kosloff. Time-dependent quantum-mechanical methods for molecular dynamics. *Journal of Physical Chemistry* **92**(8), pp. 2087–2100, 1988.

[73] E. Pijper, G. J. Kroes, R. A. Olsen, and E. J. Baerends. Reactive and diffractive scattering of H_2 from Pt(111) studied using a six-dimensional wave packet method. *Journal of Chemical Physics* **117**(12), pp. 5885–5898, 2002.

[74] H. F. Berger. Über den Einfluß des Quantenzustands auf die dissoziative Adsorption von Wasserstoff. PhD thesis. Technischen Universität Graz, 1992.

[75] D. W. Marquardt. An algorithm for least-squares estimation of nonlinear parameters. *SIAM Journal on Applied Mathematics* **11**(2), pp. 431–441, 1963.

[76] J. P. Perdew, A. Ruzsinszky, G. I. Csonka, O. A. Vydrov, G. E. Scuseria, L. A. Constantin, X. Zhou, and K. Burke. Restoring the density-gradient expansion for exchange in solids and surfaces. *Physical Review Letters* **100**(13), 136406, 2008.

[77] J. A. Rayne. Elastic constants of palladium from 4.2–300 °K. *Physical Review* **118**(6), pp. 1545–1549, 1960.

[78] D. Wetzig, M. Rutkowski, R. David, and H. Zacharias. Rotational corrugation in associative desorption of D_2 from Cu(111). *Europhysics Letters* **36**(1), pp. 31–36, 1996.

[79] J. P. Perdew, J. A. Chevary, S. H. Vosko, K. A. Jackson, M. R. Pederson, D. J. Singh, and C. Fiolhais. Atoms, molecules, solids, and surfaces: applications of the generalized gradient approximation for exchange and correlation. *Physical Review B* **46**(11), pp. 6671–6687, 1992.